creased and sometimes decreased J_P. This would seem to indicate that the net pinning force is determined by both the surface roughness and by mechanical defects, and that depending on the relative effectiveness of the etch in changing the surface condition with respect to either roughness or defects, J_P will increase or decrease.

We have also recently reported that the pinning forces are angle-dependent.[11] We believe this is due to the difference in the way in which fluxoids penetrate the surface when the angle of the field is varied. Thus the interaction of the fluxoids with the surface is again emphasized.

In order to explain the present results we note the calculations of Pearl,[12] which show that the electromagnetic region of a fluxoid spreads as the fluxoid approaches the surface, making fluxoid interactions long-range at the surface. This has the net result of stiffening the fluxoids in the surface layer and requiring that they move in unison. Pinning of fluxoids in this region is therefore enhanced. In order to initiate flux flow one must provide a force to move the fluxoids collectively. If some of the fluxoids are more strongly pinned than others, none of the fluxoids will move until a force equal to this maximum pinning force is provided. Within the volume, however, fluxoids are more flexible and flow can be initiated whenever individual fluxoids see a driving force which exceeds their pinning force. Surface pinning is therefore intrinsically more effective than volume pinning. For a given field and current density, the total driving force on a fluxoid depends on sample thickness [F_L in Eq. (1) is the Lorentz force *per unit length*]. The surface-pinning region, equal to the penetration depth in thickness, remains constant. Thus, for a given current density, the driving force on a fluxoid increases with thickness without a coincident increase in the surface-pinning force. Flux flow can therefore be initiated at a lower current density with a thick sample than with a thinner one, as we observe.

[11] W. C. H. Joiner and G. E. Kuhl, Phys. Rev. (to be published).
[12] Judea Pearl, J. Appl. Phys. 37, 4139 (1966).

PHYSICAL REVIEW VOLUME 163, NUMBER 2 10 NOVEMBER 1967

Effect of the Superconducting Energy-Gap Anisotropy on the Thermal Conductivity of Tin*

J. E. Gueths,† N. N. Clark,‡ D. Markowitz, F. V. Burckbuchler, and C. A. Reynolds
Physics Department and Institute of Materials Science, University of Connecticut, Storrs, Connecticut

(Received 9 June 1967)

Measurements of the normal- and superconducting-state thermal conductivities (K^n and K^s) were made on one pure and eleven cadmium-doped tin single crystals in the temperature range $1°<T<4°$K. Cadmium concentrations ranged from 5×10^{-3} to 0.3 at.%. The crystal orientations are tightly grouped in the near-perpendicular direction (direction of heat flow approximately perpendicular to the tin tetrad axis). The fractional change of the lattice conductivity, K_g^s, in the superconducting state and an effect in the electronic part of the conductivity K_e^s, reflecting the anisotropy of the superconducting energy gap, are studied as a function of impurity concentration. The variation of the size of the anisotropy effect with electron mean free path is found to be in reasonable agreement with the theoretical predictions of Ulbrich *et al.* and the ultrasonic attenuation results of Claiborne and Einspruch. However, the magnitude of the anisotropy effect in tin is found to be approximately twice as large as that predicted by theory. Unsuccessful attempts to bring the theoretical calculations into agreement with experiment by altering the angular features of the energy-gap function are discussed. The variation of α, the temperature coefficient of the electron-phonon scattering term in the thermal resistivity expression, was studied as a function of impurity concentration and found to increase monotonically with concentration. Also the anisotropy of β, the temperature coefficient of the impurity scattering term, is shown to be similar to that of the residual resistivity. From the measured values of the residual resistivity, ρ_0, and β's obtained from the normal-state thermal conductivities, the Lorentz number L_0 was found to be $L_{0\text{exp}}=2.49\pm0.08$ for these samples.

I. INTRODUCTION

THIS paper describes an experimental investigation of the effects of the anisotropy of the superconducting energy gap on the thermal conductivity of single crystals of dilute tin alloys. Tin was selected as the host metal for this work since it exhibits a superconducting energy-gap anisotropy suitable for detection with thermal-conductivity measurements, and single crystals in many of its dilute alloy systems are easily prepared. From recent measurements on Cd-doped tin,[1] we have learned how Cd affects some of the superconducting properties of the host metal, in particular the transition temperature, thus making it convenient to continue with Cd in an attempt to study its effect on thermal conductivity. Previous thermal-conductivity measurements were performed on poly-

* Supported by the U.S. Air Force Office of Scientific Research Grant No. AF-AFOSR-474-67 and Office of Naval Research Contract No. Nonr 2967(00).
† Present address: Wisconsin State University, Oshkosh, Wisconsin.
‡ Present address: Universidad de Costa Rica, San Jose, Costa Rica.

[1] J. E. Gueths, C. A. Reynolds, and M. A. Mitchell, Phys. Rev. 150, 346 (1966).

crystalline samples[2] or ultrapure single crystals.[3] The data presented in this paper were taken using lightly doped single crystals.

We express the normal- and superconducting-state thermal conductivities as the sum of two terms, one electronic (e) and one lattice (g), viz.,

$$\text{(normal state)} \qquad K^n=K_e^n+K_g^n, \qquad (1)$$

$$\text{(superconducting state)} \qquad K^s=K_e^s+K_g^s. \qquad (2)$$

We will frequently have occasion to refer to the ratios K^s/K^n, K_e^s/K_e^n, and K_g^s/K_g^n, which we hereafter denote as R_T, R_e, and R_g, respectively.

The theoretical work of Ulbrich, *et al.*[4] points out that, in general, a superconductor having an anisotropic energy gap will exhibit an anisotropic R_T. Making several assumptions about the nature of the anisotropic gap in tin, they proceed to calculate the anisotropic R_e for tin, and predict that its anisotropy should largely disappear for specimens having electronic mean free paths shorter than $4\xi_0$, where ξ_0 is the superconducting coherence distance. The anisotropic R_e is calculated for the case when the electronic thermal conductivities are limited by electron-impurity scattering. Direct experimental observation of this anisotropic ratio, its variation with impurity concentration, and its eventual disappearance, is difficult unless one can isolate the various terms in Eqs. (1) and (2), or contrive to make the lattice terms experimentally negligible so that $R_T \approx R_e$.

The solid solution systems are suitable for an investigation of this phenomenon. In the region of electron mean free paths for which we expect to see the effects of the anisotropic energy gap, K_g^n is vanishingly small, K_e^s is dominated by electron impurity scattering (as is K_e^n), and K_g^s is rapidly disappearing and of a nature analytically manageable. The theoretical calculation suggests that an optimum crystal orientation at which to observe the anisotropy effect and its variation with impurity content (or electronic mean free path) would be such that the direction of heat flow is perpendicular to the tin tetrad axis. It is relatively easy to satisfy this criterion, as this is the preferred growth direction for the thin cylindrical samples necessary for thermal-conductivity work.

We have selected the characteristics (e.g., orientation, impurity concentrations) of our 12 samples with all of the limitations suggested by the theoretical calculations in mind. The orientations are tightly grouped (with one exception) in the near-perpendicular direction, so that variation in R_T due to orientation effects is minimized. The range of impurity concentration was selected to obtain electron mean free paths in the region $400\xi_0 \geq l_e \geq \xi_0$. The theory does not take into account the variation in R_e due to electron-phonon scattering, but from the results of Guenault,[3] we anticipate no serious complications here, since the anisotropy effect should be evident well before significant amounts of electron-phonon scattering are present.

The specific goals of this work are: (1) to conclusively isolate an effect in the thermal conductivity of tin solid solutions which can be identified with the anisotropy of the energy gap, (2) to observe the variation of its size with impurity concentration, and (3) to compare its size with the theoretical predictions of Ulbrich *et al.*[4]

II. EXPERIMENTAL DETAILS

Spectroscopically pure (unwanted impurities $<1\times 10^{-3}$ at. %) tin and cadmium were mixed in a vacuum to prepare ingots having the desired impurity concentrations. The crystals were grown in precision bore Pyrex tubing (i.d.$=2.000\pm0.005$ mm) in a manner previously described.[1] After extraction from the tubing, the crystals were annealed for 72 h at 200°C. Slight etching in HCl enabled visual examination for macroscopic defects (slip planes, grain boundaries, inserts) and examination of orientation using an optical goniometer. θ, the angle between the tin tetrad axis and the specimen (cylindrical) axis, was determined to within $\pm1°$. Crystals of undesirable orientation or possessing macroscopic defects of a nature that might influence the experimental results were excluded from the study.

Germanium resistance thermometers, calibrated against the 1958 He vapor-pressure tables,[5] were used as temperature sensors in the thermal-conductivity measurements. Approximately 30 calibration points in the temperature interval $1<T<4.2$°K were fitted by the method of least squares to an equation of the form

$$1/T=A+B\ \ln R+C/\ln R+D(\ln R)^2+E/(\ln R)^2 \qquad (3)$$

for each thermometer. These fits, along with a deviation curve, were then used to make resistance to temperature conversions.

Two experimental arrangements were used in the course of the thermal-conductivity measurements. They are shown in Fig. 1. The arrangement in Fig. 1(a) was suitable for measurements on the lower conductivity samples. The sample and terminal strip were thermally grounded to the bath via the two copper supports. The leads from the terminal posts (No. 40 Teflon-coated copper wire) exited the can through the pumping tube after being wrapped and glued with GE 7031 cement to the copper post holding the terminal strip. The heat flowing from the top of the apparatus (at 300°K) down these leads caused the terminal and sample to run at a temperature slightly above that of the bath throughout the experiment. This tempera-

[2] G. J. Pearson, C. W. Ulbrich, J. E. Gueths, M. A. Mitchell, and C. A. Reynolds, Phys. Rev. **154**, 329 (1967).
[3] A. M. Guenault, Proc. Roy. Soc. (London) **A262**, 420 (1961).
[4] C. W. Ulbrich, D. Markowitz, R. H. Bartram, and C. A. Reynolds, Phys. Rev. **154**, 338 (1967).
[5] F. G. Brickwedde, H. van Dijh, J. R. Clement, and J. K. Logan, J. Res. Natl. Bur. Std. (U.S.) **64A**, 1 (1960).

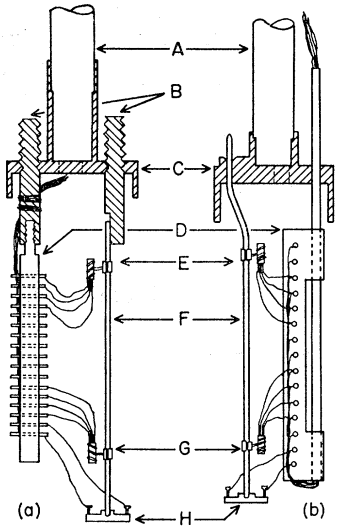

FIG. 1. The experimental chambers used for the thermal-conductivity measurements. (a) was used for the low-conductivity specimens. The electrical leads exit from the chamber via the pumping tube. (b) provides better thermal grounding and was used for the high conductivity specimens. A—Stainless steel pumping tube. B—Copper supports for the specimen and terminal strip. C—Brass can top. The copper can was soldered to the top at this point. D—Teflon terminal strip. E—Cold thermometer and mounting clamp. F—Sample. G—Hot thermometer and mounting clamp. H—Heater.

ture difference (~0.2°K), as determined by a third germanium thermometer on the terminal strip and the two thermometers on the sample, varied only slightly with bath temperature and the amount of power supplied to the sample by the heater. This situation was caused by the relatively poor thermal grounding afforded by the mechanical and glue contacts with which the specimen and terminal strip were attached to the copper supports, although low conductivity No. 40 Formvar-coated manganin wire was used to connect the thermometers and the heater to the terminal strip. As a result there were no great experimental difficulties as long as modest power inputs were required to produce temperature differences of the order of 0.1°K between the hot and cold thermometers.

The large power requirements of the purer specimens made it difficult to obtain reliable thermal conductivity data below 1.8°K, and a modified can shown in Fig. 1(b) was used. In this arrangement, the sample protruded into the bath and was soldered in place with Cerroseal solder.[6] The leads exited from the can directly into the bath through a copper tube filled with Stycast 2850 GT epoxy cement. This provided improved thermal grounding of both the specimen and terminal strip, but required a longer specimen for soldering at the can top. As a check on the reproducibility of our data, sample 7 was run on both apparatuses with no discernible difference in the data of the two runs.

The Teflon terminal strip served very well as a means of providing electrical isolation and mechanical support for the leads. Connections from the thermometers and heater to the terminal strip were made with No. 40 Formvar-coated manganin wire, which provided suitable thermal isolation of the sample. The heater (6185 Ω of 1-mil Formvar-coated manganin wire wound on a thin copper spool) was soldered to the sample. The thermometers were attached to the sample mechanically with copper clamps. Thermal contact between the clamps and the thermometers was provided by copper wire wound around the thermometers supplemented with GE 7031 cement.

The copper can (not shown in Fig. 1) was connected to the top of the sample chamber with Cerroseal solder.[6] Vacuum was maintained at 5×10^{-6} Torr as measured at the top at room temperature in the experimental chamber during the thermal-conductivity runs.

The experimental procedure was to move from 4 to 1°K while taking the superconducting-state data. Then a longitudinal magnetic field was applied to drive the sample normal. The normal-state data were then taken, along with the magnetoresistance data when necessary. With this operational sequence, the effects of trapped flux on the superconducting-state data were minimized, as the only field available for trapping was that of the earth.

Corrections were applied to the data for: (1) heat generated in the current leads to the heater, (2) heat lost by conduction along the leads from the hot thermometer and heater, and (3) small calibration shifts which the thermometers exhibited from run to run. Heat generated in the thermometers or thermometer leads and heat losses by radiation or conduction through the gas remaining in the chamber were calculated and found negligible. In addition, sample No. 1 exhibited a significant longitudinal magnetoresistance at the field value applied to the specimens to drive them normal below T_c. Using the method employed by Guenault,[3] corrections of about 32% at 1.3°K and 18% at 3.9°K were made, the average correction being 25%. The distances between the midpoints of the thermometer clamps were determined with a vernier caliper. Measurements with a traveling microscope revealed that the diameters of the specimens were equal to the i.d. of the Pyrex tubings in which they were grown.

Electrical-resistivity determinations on sections of crystal symmetrically located with respect to the thermometer clamps were made using a microvolt potentiometer (Honeywell Model 2783). Measurements made at 4.2°K are reported as ρ_0 determinations, with two exceptions. Sample Nos. 1 and 2 ($\rho_{4.2}=1.12$ and 6.67×10^{-9} Ω cm, respectively) were of sufficient purity so that the temperature-dependent resistivity at 4.2°K (0.09×10^{-9} Ω cm) [7] was subtracted from $\rho_{4.2}$ to obtain ρ_0. Resistivity determinations at 77 and 273°K were compared to values expected from previous work[1] and

[6] G. K. White, *Experimental Techniques in Low Temperature Physics* (Oxford University Press, London, 1959), p. 271.

[7] V. B. Zernov and Yu. V. Sharvin, Zh. Eksperim. i Teor. Fiz. 36, 1038 (1959) [English transl.: Soviet Phys.—JETP 9, 737 (1959)].

TABLE I. Summary of the normal-state electrical and thermal characteristics of the specimens.

Sample no.	$\rho_0(\mu\Omega$ cm)	x^a (at.%)	θ	α	β	$a=\alpha T_c^3/\beta$
1	0.00103	...	80½	4.6×10^{-4}	0.0405	0.58
2	0.00658	0.0046	76	6.3	0.262	0.12
3	0.0131	0.0092	79	9.7	0.510	0.097
4	0.0360	0.0245	72½	12.	1.43	0.043
5	0.0437	0.0310	81½	14.	1.77	0.040
6	0.0552	0.0391	81	16.	2.10	0.039
7	0.0675	0.0421	59½	...	2.78	...
8	0.0704	0.0486	75	...	2.78	...
9	0.0894	0.0631	78½	...	3.66	...
10	0.173	0.122	80½	...	7.16	...
11	0.357	0.251	78½	...	14.4	...
12	0.460	0.321	77	...	18.4	...

[a] Calculated using $\rho_{0\perp}=1.39$ (at.%) (Ref. 3).

served as a check on the goniometer-derived orientations.

III. RESULTS AND DISCUSSION

A. The Normal-State Thermal Conductivity

The heat conduction by phonons K_g^n is expected to be a small part of the total normal-state thermal conductivity for alloy specimens sufficiently pure. We therefore anticipate that K^n for our purest samples will be represented by an equation of the form

$$K^n \cong K_g^n = (\alpha T^2 + \beta/T)^{-1}, \tag{4}$$

where the αT^2 and β/T thermal resistivity terms represent the scattering of electrons by phonons and impurities, respectively. The type of behavior described

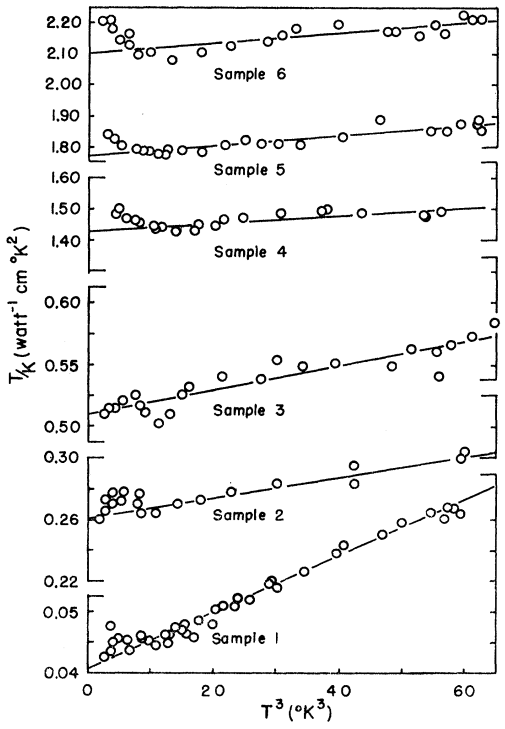

FIG. 2. T/K^n versus T^3 for the six purest specimens measured. The solid lines drawn through the data are used to determine the respective α's and β's listed in Table I for these specimens.

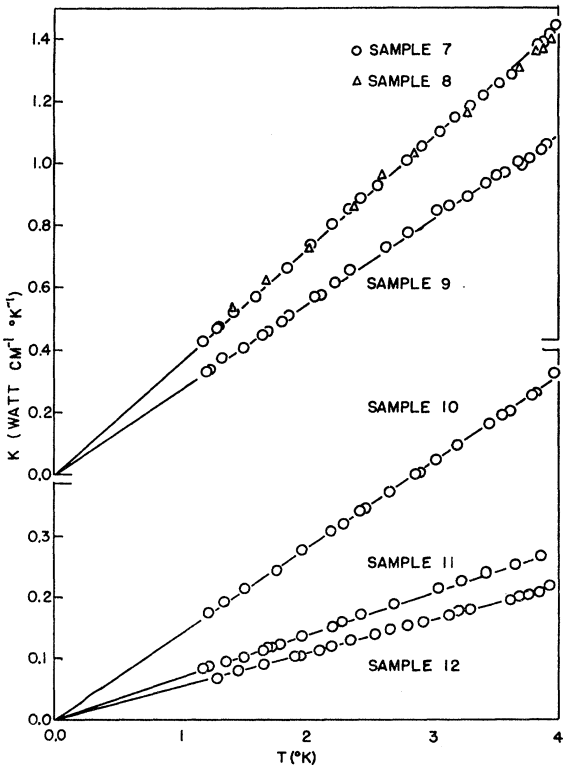

FIG. 3. K^n versus T for the specimens not shown in Fig. 2. The solid lines represent least-squares fits to the form $K^n=T/\beta$.

by Eq. (4) is detectable in samples 1–6, and plots of T/K versus T^3 for these specimens are shown in Fig. 2. We note that the data fit the form of Eq. (4) reasonably well. The values of α and β obtained from the solid lines in Fig. 2 are tabulated in Table I. Also listed are the crystal orientations θ, the electrical resistivities ρ_0, and the amount of cadmium impurity x, to be expected in crystals having these residual resistivities.[1] The calculated quantity "a" is the ratio of the thermal resistivity due to phonon scattering to that due to impurity scattering at the transition temperature ($a=\alpha T_c^3/\beta$). This parameter will be of value in the discussion of the superconducting-state thermal-conductivity data.

The samples with larger impurity concentrations (7–12) exhibit thermal conductivities that vary nearly linearly in T. This is seen in Fig. 3, and the linear K^n-T dependence suggests that impurity scattering is the only significant mechanism in these samples. There is some evidence (not noticeable in plots of the type shown in Fig. 3) for a small amount (about 3%) of lattice conductivity K_g^n at higher T values for samples 10–12.

Pearson *et al.*[2] employ an indirect method of obtaining information about K_g^n from curves of R_T versus t as a function of impurity concentration. As mentioned earlier, the small fractional size of K_g^n, even in our most impure specimens, makes a direct separation of the normal-state data into K_e^n and K_g^n unreliable. For this reason, we have subjected the data for our three most impure specimens (samples 10–12) to an analysis of the Pearson type. Their Eq. (10),

$$\ln[R_T-R_e]=\ln(R_gCT^{n-1}/L_0)+(3-n)\ln\rho_0, \quad (5)$$

assumes that: (1) $K_e^n=L_0T/\rho_0$, (2) there is no significant variation in R_e over the range of impurity concentration considered, at constant T, (3) K_g^n follows a (ρ_0, T) dependence of the universal form of Lindenfeld and Pennebaker[8]

$$\ln(K_g^n/T\rho_0)=\ln C+(n-1)\ln(T/\rho_0), \quad (6)$$

and (4) the ratio $R_g=K_g^s/K_g^n$ is a function of t independent of ρ_0 over the impurity range considered. In the present work, assumptions (1) and (2) are tested and found valid *for samples sufficiently impure so that the anisotropy effect is not altering* R_e. Although assumptions (3) and (4) have not yet been validated directly for tin alloy systems, the success that Pearson *et al.* enjoyed in interpreting their data suggests that they must be approximately correct.

Drawing straight line plots of $\ln[R_T-R_e]$ as a function of $\ln\rho_0$ similar to their Fig. 8, and employing Eqs. (5) and (6) at reduced temperatures $t=0.35$, 0.40, 0.45, and 0.50, we find a temperature dependence of K_g^n with about 2 for the exponent, the constant C having a value of 3.3×10^{-4}. With these values of n and C we obtain from Eq. (6) values of R_g that are somewhat lower (about 30%) than those predicted by the theory of Bardeen, Rickayzen, and Tewordt. As an alternative method, by making use of the expression given by Sladek[9] for K_s,

$$K_s=Tf(t)/\beta+AT^2R_g, \quad (7)$$

and Heisenberg's[10] theoretical expression

$$f(t)=2t^2/(1+t^4),$$

values of R_g were also calculated with essentially the same results as those obtained by the previous method.

The n-values obtained from the present data are significantly lower than the power dependence ($n=2.35$) indicated by the universal curve [Eq. (6)]. The range of impurity concentration and consequently the fraction of normal lattice conductivity investigated in this work are hardly large enough to warrant assigning much emphasis to this apparent disagreement or attempting to assess its implications.

It is interesting to examine the variation of the parameter α as impurities are added. Figure 4 is a plot of α versus β for all work on pure tin or dilute tin alloys known to the authors in which analyses of the type described by Eq. (4) have been made. Included are the results of Pearson,[2] Hulm,[11] Guenault,[3] and Zavaritskii.[12] One notes that the present values of α and β are consistent with those of previous investigations, and that α is monotonically increasing with impurity concentration. Behavior of this type renders quite unsatisfactory the type of separation of K^n into K_e^n and K_g^n where one assumes: (1) K_e^n is represented by Eq. (4), (2) α is independent of β, and (3) β is given by the Wiedemann–Franz law ($\beta=\rho_0/L_0$). One

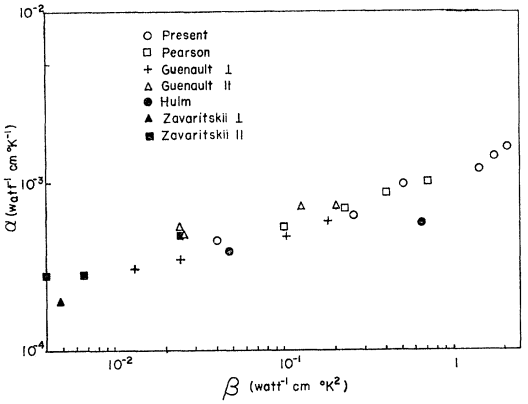

FIG. 4. α versus β. Data are included for the present specimens (Nos. 1–6) and from results of other investigations on extremely dilute tin alloys. It is clearly shown that α is not independent of impurity concentration (i.e., β) for dilute tin alloys.

[8] P. Lindenfeld and W. B. Pennebaker, Phys. Rev. **127**, 1881 (1962).

[9] R. J. Sladek, Phys. Rev. **97**, 902 (1955).
[10] W. Heisenberg, Z. Naturforsch. **3A**, 65 (1948).
[11] J. K. Hulm, Proc. Roy. Soc. (London) **A204**, 98 (1950).
[12] N. V. Zavaritskii, Zh. Eksperim. i Teor. Fiz. **39**, 1571 (1960) [English transl.: Soviet Phys.—JETP **12**, 1093 (1961)].

might suspect that this apparent $\alpha-\beta$ dependence is due to the neglect of the heat conduction by phonons, which is expected to become fractionally larger as β increases. However, the effect of a fractionally increasing K_g^n is to depress the effects of the $\alpha-\beta$ relationship in plots of the type shown in Fig. 2, and we can say that the actual $\alpha-\beta$ dependence would be even stronger than that indicated by the data in Fig. 4.

It is conventional, in normal-state thermal-conductivity analysis, to assume that β in Eq. (4) is equal to ρ_0/L_0, where $L_0=2.445\times10^{-8}$ WΩ °K^{-2} is the theoretical Lorentz number. We choose to reverse the process, and use the measured ρ_0 values and the β's determined as intercepts of the solid lines in Fig. 2 and as the slopes of the best lines (as measured by a least-squares fit) to the K-versus-T plots shown in Fig. 3. Figure 5 is a plot of $L_{\text{exp}}=\rho_0/\beta$ versus β. The error bars represent an estimate of the experimental limit of error. Using the method of least squares, the best value for L_{exp} with its standard deviation is $L_{\text{exp}}=2.49\pm0.08\times10^{-8}$ WΩ °K^{-2}. This agrees, within standard error, with the theoretical value. The fact that the crystal having the lowest θ (sample No. 7, $\theta=59\frac{1}{2}°$) exhibits a ρ_0/β value not significantly different from that obtained for crystals of higher θ ($\sim80°$) suggests that the anisotropy of β is close to that of ρ_0 ($\rho_{0\parallel}/\rho_{0\perp}=1.6$ for cadmium impurity in tin[1]).

It should be noted that the present work does not establish the anisotropy of the αT^2 term in Eq. (4). In this work, we are considering 12 specimens having nearly the same orientation, so that anisotropy effects in the normal state within the set (excepting sample No. 7) should be small.

B. The Superconducting-State Thermal Conductivity

The ratio of the thermal conductivity in the superconducting state to that in the normal state R_T, versus reduced temperature t, for all specimens, is shown in Fig. 6. The data points are obtained by dividing the superconducting-state thermal-conductivity data by a smooth curve drawn through the normal-state data. The superconducting transition temperatures were obtained by employing the measured values of $\rho_{0\perp}$ and plots of $\rho_{0\perp}$ versus T_c for the Sn-Cd dilute alloy system.[1]

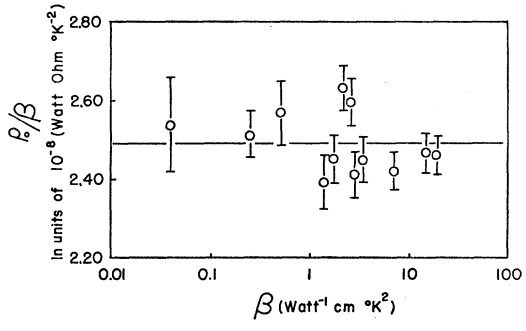

FIG. 5. Determination of the experimental Lorentz number. The solid line represents the arithmetic mean of the ρ_0/β values. It is clear that L_{exp} is constant over the range of impurity concentration investigated.

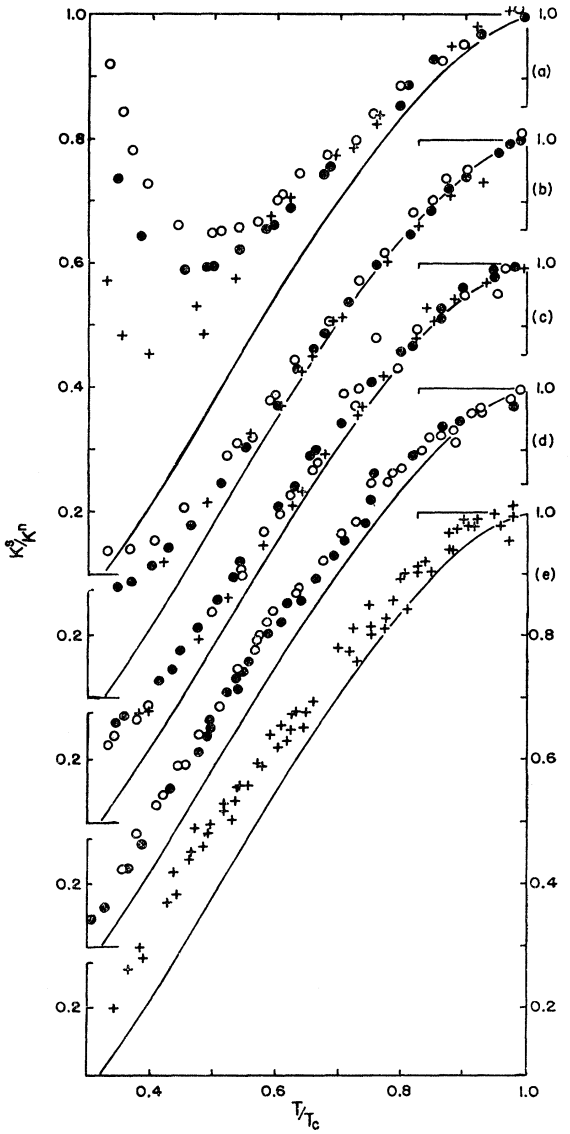

FIG. 6. $R_T=K^s/K^n$ versus t for all specimens measured in this work. The solid line is the estimated $R_e=K_e^s/K^n$ curve using $2\Delta(0)/k_BT_c=3.7$ in a calculation of the Kadanoff and Martin type. (a) (○), sample No. 12, $\beta=18.4$. (●), sample No. 11, $\beta=14.4$. (+), sample No. 10, $\beta=7.16$. (b) (○), sample No. 9, $\beta=3.66$. (●), sample No. 8, $\beta=2.78$. (+) sample No. 7, $\beta=2.78$. This set of data was used to infer the proper R_s versus t curve for *isotropic* tin. (c) (○), sample No. 6, $\beta=2.10$. (●), sample No. 5, $\beta=1.77$. (+), sample No. 4, $\beta=1.43$. (d) (○), sample No. 3, $\beta=0.51$. (●), sample No. 2, $\beta=0.262$. The anisotropy effect is evident as the upward bump in the data in the region of intermediate t. (e) (+), sample No. 1, $\beta=0.0405$. The anisotropy effect is again evident in the data for this specimen.

Studying the data in Fig. 6, we first note that purity increases as we move from top to bottom. As the impurity concentration is decreased, we observe the expected continuous suppression of the "tail" in R_T at

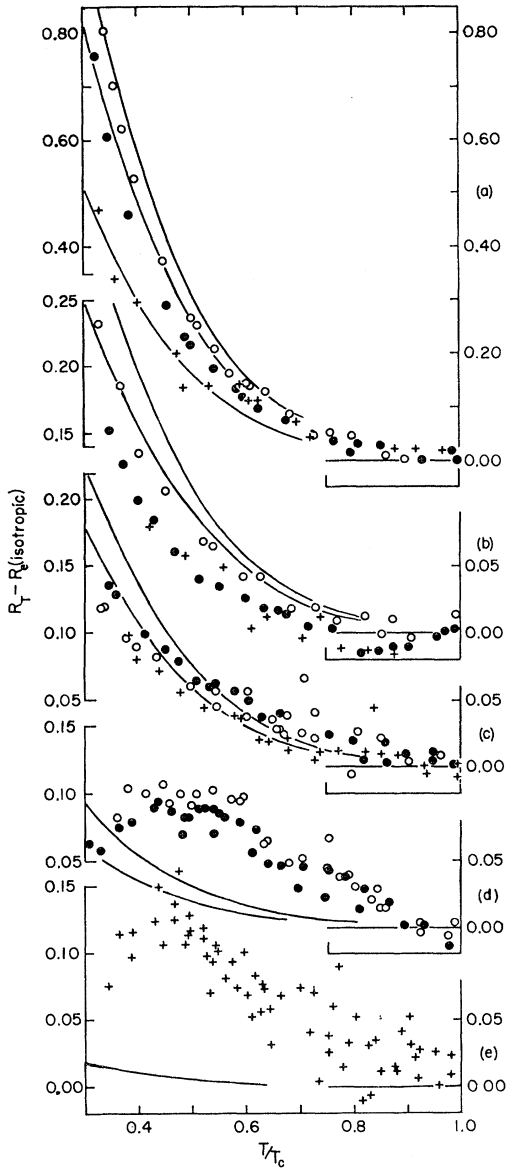

FIG. 7. $R_T - R_e$ (isotropic) versus t for all specimens measured in this work. The solid lines in each part of the Figure represent calculated estimates of this quantity using the universal curve scaled to tin for K_g^n and the values of R_g as calculated by BRT. (a) (○), sample No. 12, $\beta=18.4$. (●), sample No. 11, $\beta=14.4$. (+), sample No. 10, $\beta=7.16$. Note that the vertical scale is different for all other portions of the figure. (b) (○), sample No. 9, $\beta=3.66$. (●), sample No. 8, $\beta=2.78$. (+), sample No. 7, $\beta=2.78$. (c) (○), sample No. 6, $\beta=2.10$. (●), sample No. 5, $\beta=1.77$. (+), sample No. 4, $\beta=1.43$. A slight "bump" is perceptible at $t\approx0.7$. This marks the beginning of the anisotropy effect. (d) (○), sample No. 3, $\beta=0.51$. (●), sample No. 2, $\beta=0.262$. The anisotropy effect is now dominating the difference curve. (e) (+), sample No. 1, $\beta=0.0405$. The calculated difference (solid line) continues to decrease while the difference data continue to increase.

low-t values. The effects of lattice conduction on these curves may be gauged by following this suppression down the sequence of curves. The lattice contribution to R_T is seen to be rapidly vanishing in the regions of largest t for $\beta\approx3$. We also note that the data for the three samples in Fig. 6(b) ($\beta=3.66$, 2.78, 2.78) map smoothly onto each other in the regions of large t, suggesting that $R_T\approx R_e$ for at least the large t values. These data were then chosen as the set from which to make an estimate of the R_e-versus-t curve for the impure tin specimens.

There is another reason for choosing the data in Fig. 6(b) for estimation of the ratio R_e. Recall that the thermal-conductivity data are expected to begin reflecting the anisotropy of the superconducting energy gap at $l_e\approx4\xi_0$, which corresponds to $\beta\approx4$. Therefore, we are at an optimum position in β for the assignment of R_e: after most of the lattice component in the normal and superconducting state has disappeared, but before effects rooted in the gap anisotropy make a strong appearance. The selection of the R_e-versus-t curve for "isotropic" tin (before gap anisotropy appears) is perhaps arbitrary. Since this is "isotropic" tin, we expect that a good approximation to R_e may be obtained by employing the calculations of Kadanoff and Martin[13] (hereafter known as KM) for isotropic superconductors. As a convenient reference curve for R_e we picked the KM curve corresponding to a gap parameter $2\Delta(0)/k_BT_c=3.7$. The accepted isotropic value for tin is 3.5. However, this curve gives us both positive and negative values for the difference R_T-R_e, whereas the 3.7 gap parameter gives us positive values for all samples. This same KM curve appears in all five subplots in Fig. 6.

Proceeding through Figs. 6(c), 6(d), 6(e), we note first the still decreasing "tail" at lowest t values. In addition, in the lower two sets are seen the effects of the anisotropy of the gap on R_T. Even on these plots of raw data, the expected upward shift of R_T (caused by a shift in R_e) in the curves for $\beta=0.51$, 0.262, and 0.0405 is perceptible at intermediate t. The R_T data for our purest specimen exhibit a large amount of scatter due to difficulties encountered in measuring its very large thermal conductivities; the large number of data points, however, gives us confidence that we have an adequate representation of this curve.

It is instructive to examine the data in more detail. Figure 7 is a plot of the differences R_T-R_e (isotropic) versus t for all samples. Again the R_e (isotropic) curve which we are using is the KM calculation using a gap parameter of 3.7.

We again proceed from top to bottom. For the most impure samples we might expect that this difference can be attributed to the presence of a significant amount of K_g^s. This appears to be correct, as the data in Fig. 7(a) compare well with the solid lines, which are calculated curves of the difference

$$R_T-R_e\approx K_g^s/(K_e^n+K_g^n), \tag{8}$$

where it is assumed that $K_g^n\ll K^n$, so that $K_e^n\approx K^n$.

[13] Leo P. Kadanoff and Paul C. Martin, Phys. Rev. 124, 670 (1961).

These calculations assumed: (1) $K_e^n = L_0 T/\rho_0$, (2) K_g^n is represented by the universal curve of Lindenfeld and Pennebaker[8] scaled to tin, and (3) K_g^s is related to K_g^n by the calculations of Bardeen, Rickayzen, and Tewordt.[14] The calculated differences in the upper two sets are in qualitative agreement with, although slightly larger than, the experimental data. It then seems reasonable that the difference curves for the upper two sets be attributed to significant amounts of K_g^s present in these specimens.

Similar arguments may be made with respect to the data in Fig. 7(c). However, we do note a small but perceptible "bump" in the data in the region $t=0.7$. We also note that we are in the region of β where we expect to observe the initiation of effects caused by the gap anisotropy.[15] Continuing to Figs. 7(d) and 7(e), we see the further magnification of the anisotropy effect. The solid lines again are the anticipated shape of the difference curve via calculation, *if* this were caused by the presence of K_g^s. It is apparent that the upward shift, which we attribute to the anisotropy effect, is now dominating the difference curve.

We now wish to compare our results with the theoretical predictions of Ulbrich *et al.*[4] It is first necessary to make two corrections to the R_T-versus-t data for Figs. 7(d) and 7(e). First, we must subtract an estimate of the contribution to $R_T - R_e$ due to K_g^s/K^n, which is represented by the solid lines drawn in the figure. The difference, or portion of the respective $R_T - R_e$ data attributable to the anisotropy effect, is indicated by the smooth solid curves in Fig. 8. However, we have not yet properly taken into account the depression of R_e to be expected from scattering of electrons by phonons. This correction, which must be *added* to the solid lines of Fig. 8, can be estimated by making use of the calculations of KM. The a values necessary for this correction are obtained from the normal-state data and are listed in Table I. The only sample exhibiting an a significantly different from zero is our purest (sample No. 1). Using an approximate value ($a=0.5$) we have corrected the solid line for sample No. 1 in Fig. 8, and the net adjusted anisotropy effect for this specimen is then represented by the dashed line. The hatched line is the maximum anisotropy effect predicted by Ulbrich *et al.*[4] for tin crystals having an orientation of $\theta=80°$, which is a representative orientation for the present set of crystals. The observed anisotropy effect is more than twice the size of the maximum theoretical prediction. This discrepancy is consistent with their observation that the theory fails to explain the spread in Guenault's tin data at extremal values, between parallel and perpendicular directions, also by approximately a factor of 2.

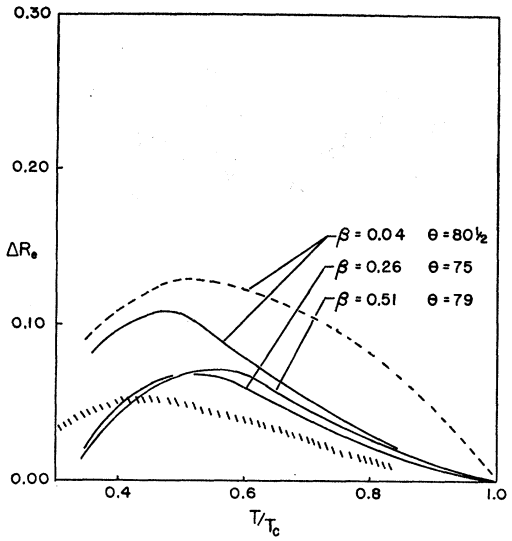

FIG. 8. Smooth curves representing the differences $[R_T - R_e(\text{isotropic})]_{\text{exptal}} - [R_T - R_e(\text{isotropic})]_{\text{calc}}$ for sample Nos. 1, 2, and 3. These curves represent ΔR_e, the change in R_e due to the anisotropy effect. The dashed line is the curve for sample No. 1 corrected to remove the suppression in ΔR_e due to electron-phonon scattering, as described in the text. The hatched line is the maximum effect predicted by Ulbrich *et al.*

An attempt was made to bring the theoretical prediction into closer agreement with our data by making changes in the gap function employed in the calculations. Two types of alteration were attempted. First, we assumed the same angular dependence of the gap parameter previously used,[4] but increased the variation so as to increase the mean-squared gap anisotropy. Second, we altered the angular dependence of the gap function in the equatorial region in a manner which gave us multiple gap values. This latter idea was suggested by recent tunneling[16] and acoustic attenuation[17] experiments on tin. Neither of the alterations assisted significantly in bringing theory into closer agreement with our data.

It is interesting to compare the "washing-out" of the gap anisotropy as evidenced in thermal conductivity measurements and in ultrasonic attenuation data of Claiborne and Einspruch.[18] To accomplish this, an indirect method had to be used once more. Values of R_e at $t=0.6$ were compared with plots of R_e against t for different values of the gap parameter $2\Delta(0)/k_B T_c$ as given by Kadanoff and Martin.[13] For the two most impure samples R_e was obtained by assuming R_g to be given by the BRT expression and setting $K_g^s = A T^2 R_e$. A was determined from a least-squares fit to an equa-

[14] J. Bardeen, G. Rickayzen, and L. Tewordt, Phys. Rev. **113**, 982 (1959).

[15] Although the electronic mean free path is slightly larger than $4\xi_0$, we expect the anisotropy effect to vary very slowly with decreasing mean free path in this region (see Fig. 2 of Ref. 4).

[16] N. V. Zavaritskii, Zh. Eksperim. i Teor. Fiz. **48**, 837 (1965) [English transl.: Soviet Phys.—JETP **21**, 557 (1965)].

[17] Lewis T. Claiborne and Norman G. Einspruch, Phys. Rev. Letters **15**, 862 (1965).

[18] Lewis T. Claiborne and Norman G. Einspruch, Phys. Rev. **151**, 229 (1966). (The resistivity ratio axis of their Fig. 5 should read 14×10^{-3} instead of 14×10^{-2}, confirmed in private communication with the authors.)

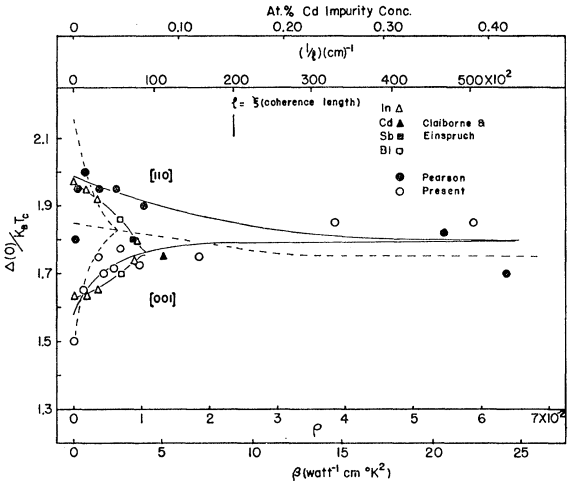

FIG. 9. Comparison of the present data with those of Claiborne and Einspruch and Pearson *et al.*, by means of a plot of the experimentally determined values of the gap parameter as a function of resistivity ratio. The solid lines are the best curves through the data and the dotted lines are the theoretical curves of Hohenberg. Error bars have been omitted for the sake of clarity. Also shown are values of the impurity concentration for cadmium-doped samples, inverse mean free path, and temperature coefficient of impurity-scattering term.

tion of the form $K_n = T/\beta + AT^2$. K_e^s was then obtained by subtracting K_g^s from the measured value of K^s. K_e^n is given by T/β. For all other samples the impurity concentration was low enough so that the approximation $R_T \approx R_e$ could be made. To determine the gap parameter, $\alpha T_c^3/\beta = a$ was taken to be zero for all samples, except for the nominally pure, for which it equals 0.54.

Figure 9 shows a plot of the gap parameter inferred in this manner coupled with that of Pearson *et al.*,[2] together with the ultrasonic attenuation results of Claiborne and Einspruch.[18] The results are stated in the form of an effective average gap (in units of $k_B T_c$) plotted as a function of the resistivity ratio ρ. The impurity concentration, inverse mean free path, and β scales were drawn using the approximate proportionality between these parameters and the residual resistivity of the present work. We compare the value of ρ where the anisotropy washes out for both experiment and theory. As can be seen, excellent qualitative agreement is realized. Claiborne and Einspruch took their measurements with the phonon wave vector parallel to the [110], [100], and [001] directions as shown. The thermal-conductivity curves also show the shape predicted by Hohenberg[19]; the "washing-out" of gap anisotropy occurs at about the impurity concentration that is theoretically expected. The fact that Pearson's nominally pure sample is out of line with the rest of his samples is probably due to an orientation effect; this particular crystal may be a high angle one compared with his other samples. The shape of the ultrasonic attenuation curves is different from that to be expected from Hohenberg's theory, but this may be attributable to inaccuracies in the resistivity-ratio measurements or to the fact that in each type of experiment the averaging of the gap is different. It is to be noted also that the value of the gap at zero impurity concentration is in reasonable agreement with estimates of the gap in directions almost parallel and perpendicular to the tetrad axis, made from tunneling data.

[19] P. Hohenberg, Zh. Eksperim. i Teor. Fiz. **45**, 1208 (1963) [English transl.: Soviet Phys.—JETP **18**, 834 (1964)].

IV. CONCLUSION

We have isolated an effect in the thermal-conductivity ratio which can be identified as reflecting the anisotropy of the superconducting energy gap in tin. As expected, its magnitude is found to be a function of electron mean free path. Good agreement is found between the value of the mean free path at which the anisotropy effect disappears and the theoretical predictions of Ulbrich *et al.* In addition, the point at which the anisotropy is effectively washed out agrees well with that observed by Claiborne and Einspruch with their ultrasonic attenuation measurements on dilute tin alloys. However, the magnitude of the effect is found to be approximately twice as large as the theoretical prediction. This is consistent with the inability of the theory to explain (by about a factor of 2) the magnitude of the spread in the thermal-conductivity ratios between parallel and perpendicular directions in pure tin measured by Guenault. By plotting values of α, as determined by a number of investigators, as a function of β, we have found α to increase monotonically with impurity concentration, and from plots of β against experimentally determined values of the Lorentz number, we have shown that the anisotropy of β is close to that of ρ_0. Experimentally, the Lorentz number was found to be $L_{\text{exp}} = 2.49 \pm 0.08$.

ACKNOWLEDGMENTS

The authors are indebted to M. Mitchell and P. Garbarino for assistance in performing the calculations and to H. Taylor for technical assistance.

The computational part of this work was carried out in the Computer Center at the University of Connecticut, which is supported in part by Grant No. GP-1819 of the National Science Foundation.